https://doi.org/10.5194/wes-2023-180
Preprint. Discussion started: 16 January 2024

eawe european academy of wind energy
Open Access WIND ENERGY SCIENCE DISCUSSIONS

The potential of wave feedforward control for floating wind turbines: A wave tank experiment

Amr Hegazy[1], Peter Naaijen[2], Vincent Leroy[3], Félicien Bonnefoy[3], Yves Pérignon[3], and Jan-Willem van Wingerden[1]

[1]Delft Center for Systems and Control, Delft University of Technology, Mekelweg 2, 2628 CD, Delft, The Netherlands
[2]Maritime and Transport Technology, Delft University of Technology, Mekelweg 2, 2628 CD, Delft, The Netherlands
[3]Nantes Université, École Centrale de Nantes, CNRS, LHEEA, UMR 6598, F-44000 Nantes, France

Correspondence: Amr Hegazy (a.r.hegazy@tudelft.nl)

Abstract. Floating wind energy has attracted substantial interest since it enables the deployment of renewable wind energy in deeper waters. Compared to the bottom-fixed turbines, floating wind turbines are subjected to more disturbances, predominantly from waves acting on the platform. Wave disturbances cause undesired oscillations in rotor speed and increase structural loading. This paper focuses on investigating the potential of using wave preview measurement in the controller system labeled as wave feedforward control. Two wave feedforward controllers were designed: one to reduce generator power oscillations, and the other one to minimize the platform pitch motion. In this study, a software-in-the-loop wave tank experiment is presented for the purpose of investigating the potential of wave feedforward control for floating wind turbines. In the experiment, a 1:40 scaled model of the DTU 10 MW reference wind turbine is used on top of a spar platform, with the reference closed-loop functionalities. Different environmental conditions, including wind speed, significant wave height, turbulence intensity and wave spreading, were applied during the experiments to test the control performance, and their effect on the turbine dynamics in general. It was found that the feedforward controller for rotor speed reduces the power fluctuations properly with a fair control effort, while the one for platform pitch motion requires huge actuation duty. It was concluded that wind turbulence has more dominance on the global dynamic response than waves.

1 Introduction

Wind energy is pivotal for meeting the decarbonisation objectives of the European Union (EU) energy system, as it ensures delivering clean, affordable and secure electricity to various sectors; including households, industry and transport. Consequently, wind energy is expected to heavily contribute to the EU renewable energy targets. This is not surprising, especially when we know that in 2022, wind energy covered 16% of the EU electricity demand and accounted for ~~over one third (~~37%~~)~~ of the total electricity generated from renewable sources in the EU in 2021. No wonder the EU is regarded as a pioneer in wind energy. Accordingly, this has seen the EU revising the renewable energy directive, which lays down a minimum binding target of 42.5% share of renewables by 2030 with an aspiration to reach 45%. This is 10.5% higher than the initial 32% target. Subsequently, the EU could fulfill its ambition of becoming climate-neutral by 2050 (European Commission, 2023).

https://doi.org/10.5194/wes-2023-180
Preprint. Discussion started: 16 January 2024

eawe european academy of wind energy
Open Access WIND ENERGY SCIENCE DISCUSSIONS

Offshore wind is quite superior to onshore wind when it comes to the higher wind speeds and consistency in direction. Floating offshore wind, in particular, offers unique opportunities for Europe, as FOWTs can produce electricity further offshore and in deeper waters than bottom-fixed turbines, which opens the door for offshore wind development in countries with deeper sea basins such as the Mediterranean and Atlantic. Nevertheless, floating offshore wind turbines operate in rough environmental conditions. As opposed to onshore turbines, waves come into play and act as another source of disturbances affecting the wind turbine, and exerting extra structural loading on top of the loads due to wind turbulence. Consequently, fatigue loads experienced by FOWTs are increased due to the contribution added by the waves (Saenz-Aguirre et al., 2022). FOWTs come with additional challenges compared to their onshore counterpart from a control point of view, as extra dynamics introduced by the floating platform make the control problem more complex. A well-known example is the negative damping instability that forces a reduction in the bandwidth of the feedback pitch controller below the platform pitch eigenfrequency (Jonkman, 2008; van der Veen et al., 2012; Fischer, 2013; Lemmer et al., 2020; Hegazy et al., 2023a). As a result, the blade pitch feedback controller has limited authority against errors occurring due to disturbances such as wind and waves, which results in slower control action in response to disturbances. As mentioned before, wind and waves are the main sources of disturbance affecting FOWTs. If a preview of those disturbances exists, it can be exploited within a feedforward control framework to combat ~~such disturbances~~. This would reduce the control effort exerted by the feedback controller, as it would not need to react to disturbances anymore since the feedforward would be taking care of them. As for wind disturbance, nacelle-mounted Light Detection And Ranging (LiDAR) technology can provide measurements of the upstream wind inflow, from which, an estimate of the rotor-effective wind speed is obtained, which ~~is~~ then can be used for ~~FeedForward~~ (FF) wind turbine control. LiDAR FF control has proven its ability to reduce fatigue loads and power excursions effectively (Schlipf et al., 2013; Navalkar et al., 2015; Schlipf et al., 2020), which helped boost its momentum towards commercialisation.

https://doi.org/10.5194/wes-2023-180
Preprint. Discussion started: 16 January 2024

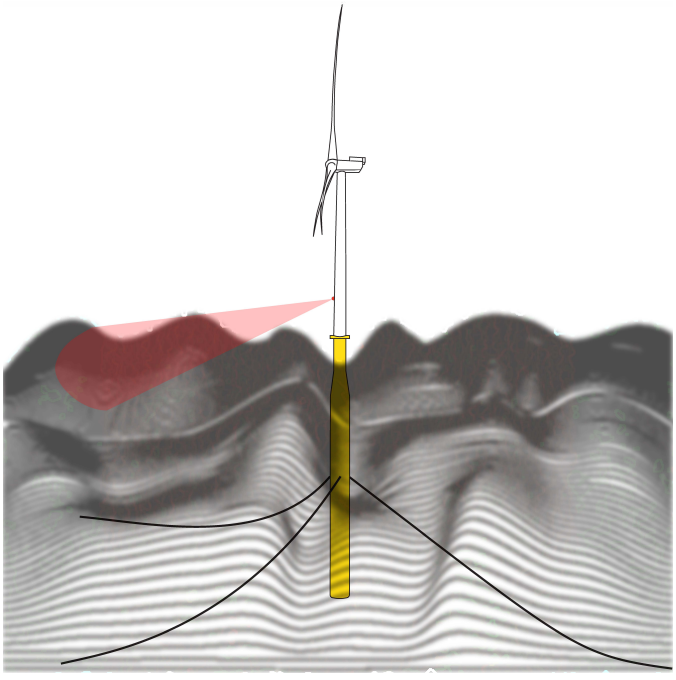

Figure 1. Schematic of the wave feedforward control strategy. The feedforward control action is based on the wave elevation measured by a radar upstream of the wind turbine. This measurement is used to obtain a preview of the wave excitation forces at the floating platform ahead of time, which is the input to the wave feedforward controller.

Generally speaking, wave FF control strategy resembles LiDAR FF control, as in the case of wave FF, a preview of the wave height/loads is acquired based on measurements of the surrounding upstream waves, as shown in Fig. 1, which is then exploited within the turbine controller. In this regard, several technologies are available to measure the surface wave elevation such as: wave buoys, radars, or satellites. The radar technology, in particular, has the capability of scanning large areas at further distances which makes it attractive (Fontanella et al., 2021). Predictions of the surface wave elevation can then be established from the radar images of the wave field (Naaijen and Wijaya, 2014). Kim et al. (2023) developed a phase-resolved ocean wave predictions algorithm to incorporate directional sea states and validated them against dedicated scaled wave tank experiments, considering sea states with different directional spreading as well as different wave steepness. Later on, they continued the development of the prediction algorithms with the aim of enhancing the accuracy of continuous wave prediction as discussed in Kim et al. (2024a). Furthermore, Kim et al. (2024b) proposed wave excitation force prediction methods, where they validated the prediction algorithms against the experimental data.

Wave FF, however, is not yet as mature as LiDAR FF, since it is not thoroughly discussed in the literature. Only a few studies investigated the subject as in Raach et al. (2014) where a Non-linear Model Predictive Control (NMPC) strategy was developed, considering perfect wind/wave preview~~,~~ demonstrating promising improvement over the baseline feedback controller with regard to blade loads, but the contribution of each of the LiDAR and wave FF separately was not clarified. In Ma et al. (2018), an effective deterministic finite-horizon LQR controller was designed, exploiting a real-time forecast of

https://doi.org/10.5194/wes-2023-180
Preprint. Discussion started: 16 January 2024

eawe european academy of wind energy
Open Access WIND ENERGY SCIENCE DISCUSSIONS

the wave loads, to reduce tower-base fore-aft (FA) bending moment, and achieved assorted results. A model-inversion wave FF controller utilizing a preview of the incoming wave elevation, with the objective of reducing rotor speed oscillations, was developed in Fontanella et al. (2021) and Al et al. (2020) considering a few degrees of freedom corresponding to the global dynamics of the FOWT, where the FF controller was added to the standard feedback (FB) controller to improve power quality by reducing the rotor speed fluctuations caused by waves. They showed that the controller could alleviate the effects of the wave disturbance on the rotor speed, hence, the generator power, with a positive side-effect of lowering the fatigue loads for the Low-Speed Shaft (LSS) and blades.

Unlike the model-based ~~control~~ used in Fontanella et al. (2021); Al et al. (2020) for the control synthesis, Hegazy et al. (2023b) employed a data-driven control approach that can capture the missing dynamics that are not considered in the model-based one. ~~As t~~he Predictor-Based Subspace Identification (PBSID$_{opt}$) algorithm van der Veen et al. (2013) was used to develop the wave FF controllers, which were synthesised for the same two control objectives discussed in this study; power regulation, and platform pitch motion reduction. Those controllers were then tested in the aero-servo-hydro-elastic simulation suite, Qblade (Marten, 2023). Hegazy et al. (2023b) went on to show that FF control for power regulation helps reduce the rotor speed fluctuations, and thus, lead to higher power quality output. Meanwhile, the FF control for platform pitch mitigation requires huge control effort.

A step forward towards pushing the technology readiness level of ~~such~~ control strategy would be conducting physical experiments. Such experiments can be performed in the field using a full-scale prototype, or scaled-model of the system can be tested either in a wind tunnel or a wave tank. Scaled-model testing helps to better understand the system dynamics, and at a lower cost than full-scale prototypes. Whether the scaled-model testing is conducted in a wind tunnel or a wave basin, defines the complexity level of the physical scale model of the FOWT. If the tests are performed in a wind tunnel, the part of the FOWT with the uncertain theoretical model is reproduced with a physical scale model, while a numerical model is used to emulate the rest of the FOWT. ~~Both t~~he physical and the numerical models are then coupled via continuous measurement of some quantities of the physical model and actuation of other quantities computed in the numerical model (Fontanella et al., 2023). Meanwhile for wave tank testing, a numerical model is used to define the turbine aerodynamics and control actions, while the hydrodynamic and structural response of the platform is reproduced with a physical scale model (Chen et al., 2022).

Within the context of FF control of wind turbines, field tests of full-scale prototypes were conducted to investigate the effectiveness of LiDAR FF wind turbine control, which confirmed the positive impact LiDAR FF control has with regard to power regulation, and structural loading as was reported in Scholbrock et al. (2013) and Schlipf et al. (2014). When it comes to wave FF control, a single experimental campaign was performed in the wave basin at MARIN to validate the model-based wave FF controllers developed in (Al et al., 2020). Unfortunately, the experiments were not successful due to unknown reasons that have nothing to do with the FF controller itself (Al, 2020). So to the best of the authors' knowledge, no successful experiments have been conducted for the purpose of investigating wave FF control potential so far. This takes us to the main contributions of this article:

- Explore the potential of wave FF control strategy by conducting scaled-model testing in a wave basin.

https://doi.org/10.5194/wes-2023-180
Preprint. Discussion started: 16 January 2024

– Investigate the effect of different environmental conditions on the performance of the different wave FF controllers.

The remainder of this article is structured as follows: Section 2 presents the experimental setup of the model-scale test. Afterwards, the control design procedure is discussed in Section 3. Results from the conducted wave tank scale-model tests are then discussed in Section 4. Finally, Section 5 ~~will draw~~ the conclusion.

2 Experimental Setup

The experimental campaign was performed in the Hydrodynamic and Ocean Engineering Wave Tank of École Centrale de Nantes (ECN) in France. It is 50 m long, 30 m wide and 5 m deep, equipped with a segmented wave maker composed of 48 independent flaps distributed over the width of the basin, which enables generating high quality waves. It can produce both regular and irregular waves taking into account wave direction. Both uni-and-multi-directional waves can be generated. The generated wave periods can vary from 0.5 to 5 s, while the significant wave height at model scale can go up to 1 m for regular waves, and 0.6 m for irregular ones.

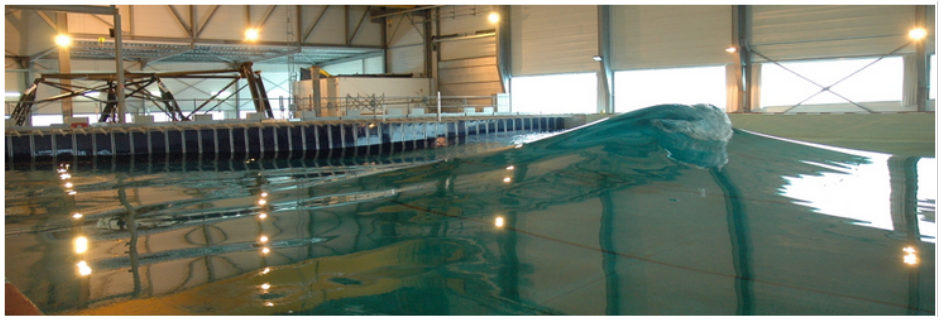

Figure 2. Hydrodynamics and Ocean Engineering Tank at École Centrale de Nantes.

2.1 Floating wind turbine model

For this study, the DTU 10 MW Reference Wind Turbine (RWT) (Bak et al., 2013) mounted on top of a spar-type floater as shown in Fig. 3~~.~~ The floating platform was designed at ECN within the context of the SOFTWIND project (Arnal, 2020). The Softwind floating platform is a spar-type floater. It is of 90 m draft and 18 m diameter, tapered to 11.2 m diameter at the water level. The mooring system ~~considered~~ is composed of three catenary lines contained within a 16 m radius with a 120° spacing. Each line is fixed on two fairlead points by means of delta connection lines to ensure high yaw stiffness. The parameters of both the DTU 10 MW RWT and the Softwind floating platform are shown in Table 1 and Table 2, respectively.

The floating wind turbine is regulated with an industry-standard generator-speed controller, as at below-rated wind speeds, the controller is seeking to maximize the extracted power by keeping the collective blade pitch angle, θ_c, constant while varying the generator torque, τ_g, as a function of the square of the generator speed, ω_g, as follows:

$$\tau_g = k_g \omega_g^2, \tag{1}$$

https://doi.org/10.5194/wes-2023-180
Preprint. Discussion started: 16 January 2024

eawe european academy of wind energy
Open Access WIND ENERGY SCIENCE DISCUSSIONS

with $k_g = 0.5\rho\pi r^2(C_{p,max}/\eta_g^3\lambda_{opt}^3)$, being the generator-torque constant, ρ is the air density, r is the rotor radius, and η_g is the gearbox ratio. $C_{p,max}$ is the maximum power coefficient, which is achieved at the optimal tip-speed ratio, λ_{opt}, and zero blade pitch angle.

At above-rated wind speeds, the controller regulates the generator speed to its rated value, while keeping the generator torque constant at its rated value. As a result, generator power fluctuations are directly proportional to the oscillations occurring in the generator speed. The collective blade pitch controller regulates the generator speed about its rated value, $\omega_{g,rat}$, according to the following feedback control law:

$$\theta_c = k_p(\omega_g - \omega_{g,rat}) + k_i \int (\omega_g - \omega_{g,rat})dt, \tag{2}$$

where k_p and k_i are the proportional and integral gains respectively, which were properly tuned using loop-shaping technique. The feedback controller is considered the baseline against which the potential of the wave FF controller is evaluated.

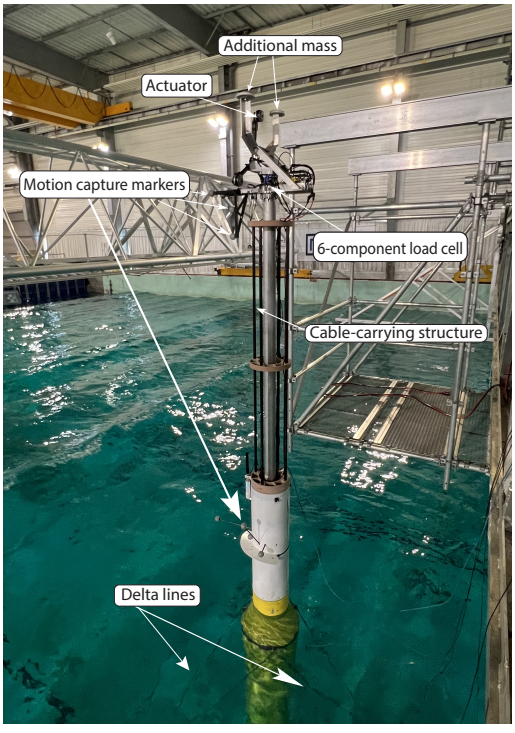

(a)

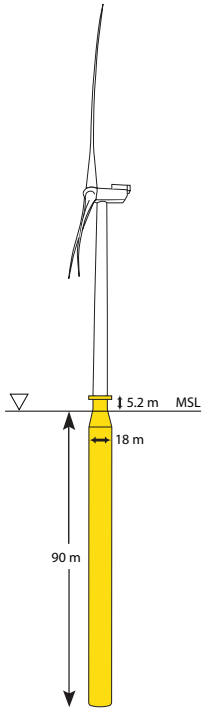

(b)

Figure 3. The floating wind turbine 1:40 scaled model of the DTU 10 MW RWT on top of the SoftWind Spar.

https://doi.org/10.5194/wes-2023-180
Preprint. Discussion started: 16 January 2024

eawe european academy of wind energy
Open Access WIND ENERGY SCIENCE DISCUSSIONS

Table 1. Key parameters of the SOFTWIND spar platform (Arnal, 2020).

Parameter	Value	Unit
Mass	1.94×10^7	kg
Roll inertia about CoG FOWT	10^{10}	kg.m^2
Pitch inertia about CoG FOWT	10^{10}	kg.m^2
Yaw inertia about CoG FOWT	6×10^8	kg.m^2
Draft	90	m
Spar diameter	18	m

Table 2. Key parameters of the DTU 10 MW RWT (Bak et al., 2013).

Parameter	Value	Unit
Cut-in wind speed	4	m/s
Cut-out wind speed	25	m/s
Rated wind speed	11.4	m/s
Rated power	10	MW
Peak power coefficient	0.48	-
Optimal tip speed ratio	7.55	-
Rotor diameter	178.3	m
Hub Height	119	m
Minimum rotor speed	6	rpm
Maximum rotor speed	9.6	rpm
Rotor mass	227,962	kg
Nacelle mass	446,036	kg
Tower mass	628,442	kg

2.2 Measurements

The measurement system consists of several sensors. As for the forces and moments, two six-component load cells (model HBM-MCS10) are placed along the tower. The first is installed between the tower-top and the nacelle to measures the rotor integral forces and torques, while the second is installed at the transition piece to measure the tower-base bending moments. The axial load in the mooring lines is measured through an in-line submersible one-component load cell located at the connection

https://doi.org/10.5194/wes-2023-180
Preprint. Discussion started: 16 January 2024

between the main-line and the delta-line where the tension is supposed to be maximum. Four strain gauges are installed at the tower base to measure the tower deformation bending strain.

An accelerometer of model ASC 5525MF-002 is installed on the nacelle, above the load cell at the tower-top. This accelerometer is used to compute the inertial force and the weight terms that should be removed from the measured force to obtain the actual thrust forces.

Regarding motions, an optical Qualisys motion capture system is used to measure the 3D position of 8 spherical reflective markers (see Fig. 3). Four markers are fixed to the nacelle to measure the tower-top motion, while another four markers are fixed to the platform top to measure the platform motion. The platform and nacelle velocities ~~can then be~~ derived from the positions measured by the motion capture system via an implicit super-twisting differentiator. The numerical simulation running in parallel to the experiments uses the platform and nacelle velocities as input for the computation of relative velocities on the elements of the blades.

Moreover, seven wave gauges, required for the wave reconstruction and prediction algorithm, are installed at different locations in the wave basin. The waves were calibrated with one wave probe exactly at the model's equilibrium position.

All the onb~~o~~oard sensors' signals are acquired via CompactRio data acquisition system, which is installed inside the spar platform to record all the measurements of the sensors fixed on the FOWT model. An HBM Quantum signal-conditioning unit records the data from the mooring load cells, the wave gauges and the water temperature sensor through the Catman software. The Qualisys software records the FOWT motions on a PC. An Ethernet cable connects the PC with the CompactRio in order to ensure the fastest possible data exchange. These three systems are then synchronized via a trigger signal generated at the start of the wavemaker.

2.3 Software-In-the-Loop system

The main purpose of the Software-In-the-Loop (SIL) system is to take care of reproducing the aerodynamic loads on the FOWT model. The SIL system depends on a real-time loop that runs the acquisition and the numerical simulation alongside the physical model testing. A motion tracking system measures the position of the platform (reference point: platform top, or tower base) and the tower top deflection (fore-aft and side-side), whenever the model reacts physically to external loads (gravity, waves, moorings, and actuator). A set of differentiators are then used to calculate the velocity. Once the displacements and the velocities are measured, they are provided to OpenFAST as inputs to calculate the thrust force acting on the rotor. By applying Froude scaling on the thrust force obtained from OpenFAST, the reference force to apply with the actuator is then derived at model scale and ~~apply~~ by a set of thrusters. The inner loop ~~consists of the actuator and~~ implicit sliding mode control which aims at reproducing as fast and accurate as possible the axial thrust force~~.~~

https://doi.org/10.5194/wes-2023-180
Preprint. Discussion started: 16 January 2024

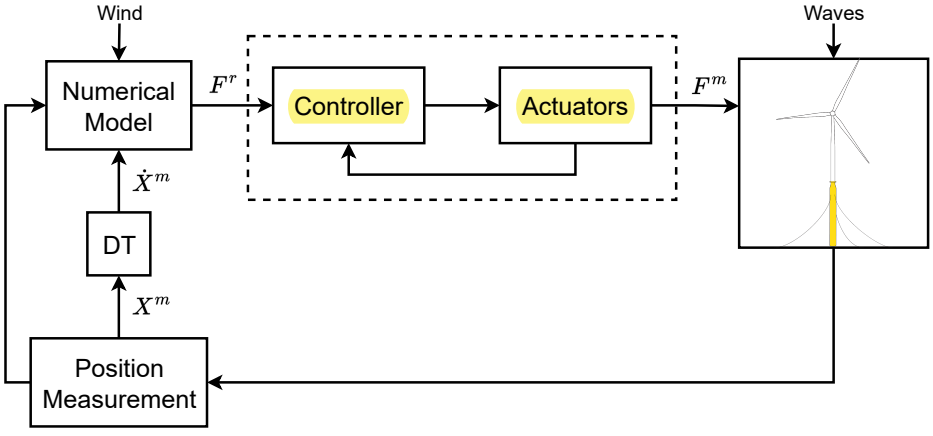

Figure 4. Scheme of the real-time loop for the SoftWind SIL approach.

2.4 Wave prediction

Regarding the preview of the wave excitation forces, a real-time phase-resolved ocean wave forecasting algorithm, developed by Kim et al. (2023, 2024a), was used. It is composed of two steps: (1) reconstruction of the initial wave conditions by assimilating data from observations; (2) wave propagation to achieve wave preview by simulating wave surfaces over a specific zone in the spatio-temporal domain. Once the wave preview is available, the wave excitation force estimation methods in Kim et al. (2024b) are applied to predict the wave excitation forces acting on the FOWT.

Figure 5 illustrates the comparison between the real surface wave elevation at the FOWT and the predicted wave elevation expected at the FOWT. We can already see that the prediction algorithm can provide a fairly accurate wave preview. ~~For more details about the prediction algorithm, the reader is referred to (Kim et al., 2023, 2024a, b).~~

https://doi.org/10.5194/wes-2023-180
Preprint. Discussion started: 16 January 2024

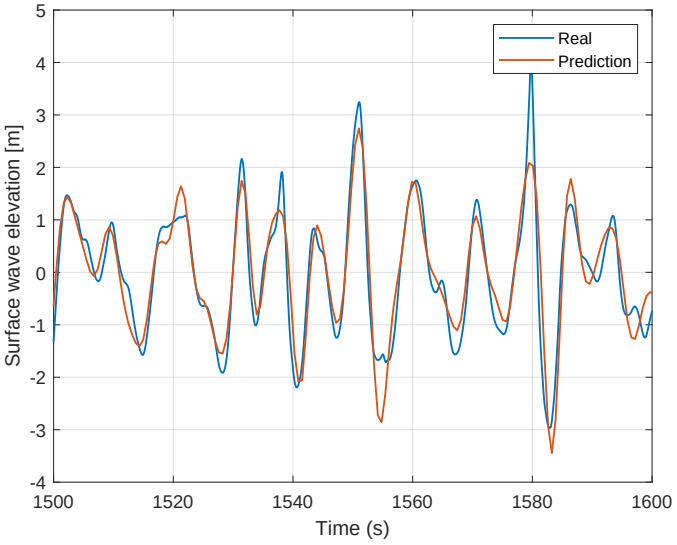

Figure 5. Comparison between the wave preview, obtained via the prediction algorithm (Kim et al., 2023), and the wave at the FOWT location.

3 The control model

In this section the controller design is presented. First, the control model is explained before dwelling on the control synthesis of the FF controller.

3.1 Data-driven approach

Figure 6 shows a block diagram of the FOWT model and control signals. Each block represents a linear Transfer Function (TF). G_{θ_p,M_w} represents the mapping from the wave-induced pitch moments, M_w, to the platform pitch motion, θ_p, while G_{ω_g,M_w} maps the wave-induced pitch moments to the generator speed, ω_g. Similar to the wave moment, the effect of blade pitch on generator speed and platform pitch motion is described by the TFs $G_{\omega_g,\beta}$ and $G_{\theta_p,\beta}$, respectively.

To obtain these TFs, which are required for the control design, identification is conducted on the results obtained from QBlade (Marten, 2023). QBlade is a fully coupled, non-linear, aero-hydro-servo-elastic wind turbine simulation suite that is capable of simulating wind turbines with a good level of accuracy. System identification is also required when using QBlade for control design purposes, as it is not equipped with a linearization functionality, and thus, making it complicated to do model-based control.

https://doi.org/10.5194/wes-2023-180
Preprint. Discussion started: 16 January 2024

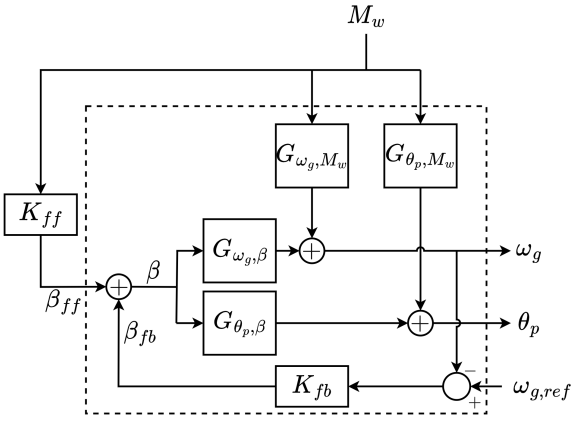

Figure 6. Block diagram of the FOWT model

The TFs were identified at an average wind speed of 16 [m/s] as an operating point. A similar procedure was used for both the spectral estimation, and the system identification, where an experiment of duration of 25000 [s] was performed in QBlade.

In order to obtain the TFs; $G_{\omega_g,\beta}(s)$ and $G_{\theta_p,\beta}(s)$, a chirp signal, logarithmically distributed over the experiment's duration, was used to excite β within a frequency band (0.02 to 0.3 Hz). As for $G_{\omega_g,M_w}(s)$ and $G_{\theta_p,M_w}(s)$, a JONSWAP spectrum was used ~~to excite the system~~.

A non-parametric form of the above-mentioned TFs ~~can be~~ obtained from the input-output data by spectral estimation. A frequency response function (FRF), assuming no correlation between the input and noise signals, ~~can be~~ achieved according to:

$$G_{y,u}(j\omega) = \frac{S_{yu}(j\omega)}{S_{uu}(j\omega)}, \tag{3}$$

where ω in Eq. (3) denotes the frequency, $j = \sqrt{-1}$, while $S_{yu}(j\omega)$ is the cross-power spectral density of the output and input, $S_{uu}(j\omega)$ is the auto-power spectral density, and $G_{y,u}(j\omega)$ represents the estimated FRF. Based on the estimated frequency response functions and the feedforward structure given in Fig. 6 the optimal non-parametric feedforward controller, for both the generator speed control and the platform pitch motion control, can be estimated and are respectively given by:

$$K_{ff,\omega}(j\omega) = -\frac{G_{\omega_g,M_w}(j\omega)}{G_{\omega_g,\beta}(j\omega)}, \tag{4}$$

$$K_{ff,\theta_p}(j\omega) = -\frac{G_{\theta_p,M_w}(j\omega)}{G_{\theta_p,\beta}(j\omega)}. \tag{5}$$

The optimal non-parametric controllers are given by the blue lines in Fig. 7 and Fig. 8, respectively.

So far, the controllers given in Eq. (5) were ~~obtained using~~ non-parametric since FRFs were used. However, they cannot be directly employed for control implementation.

https://doi.org/10.5194/wes-2023-180
Preprint. Discussion started: 16 January 2024

eawe european academy of wind energy
Open Access WIND ENERGY SCIENCE DISCUSSIONS

The parametric controllers are obtained by fitting stable FF parametric TFs to ~~the~~ spectral estimate as shown in Fig. 7 and Fig. 8. The fitting must be ensured to be of the highest accuracy within the wave band enclosed by the dashed vertical lines in the figures. Outside the wave bandwidth, the controller is not supposed to react.

The parametric wave FF targeting the power regulation, K_{ff,ω_g}, takes a structure that is a combination of a double integrator, first order zero, and a second-order system according to Eqn. 6:

$$K_{ff,\omega_g} = \frac{K_{\omega_g}}{s^2} \frac{\tau s + 1}{s^2 + 2\zeta\omega_c s + \omega_c^2}, \tag{6}$$

where K_{ω_g} is a static gain for controller tuning, τ a time constant, ζ the damping ratio, and ω_c being the corner frequency of the controller.

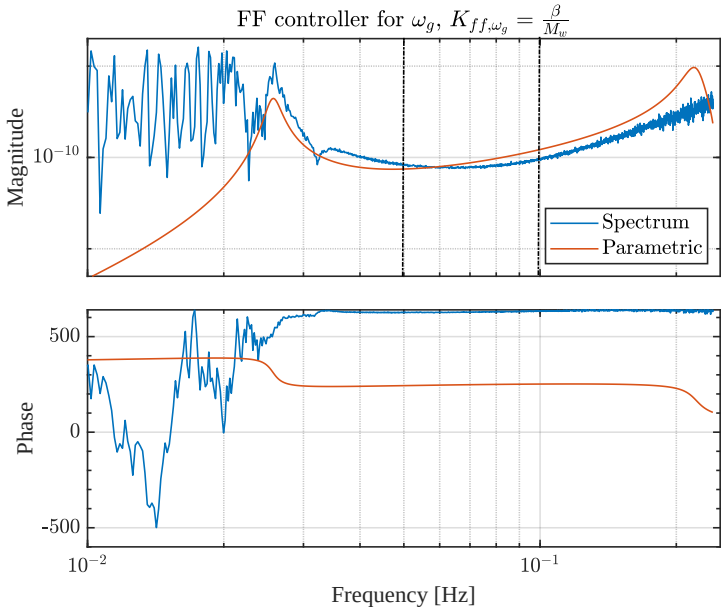

Figure 7. Bode plot of the optimal feedforward controller that targets the high speed shaft rotor speed. Blue: spectral estimate, Red: parametric controller.

While for the parametric FF controller targeting the platform pitch, K_{ff,θ_p}, the controller structure is composed of a double differentiator together with a second order system, with K_{θ_p} being a static gain for controller tuning, as illustrated in Eqn. 7:

$$K_{ff,\theta_p} = \frac{K_{\theta_p} s^2}{s^2 + 2\zeta\omega_c s + \omega_c^2} \tag{7}$$

https://doi.org/10.5194/wes-2023-180
Preprint. Discussion started: 16 January 2024

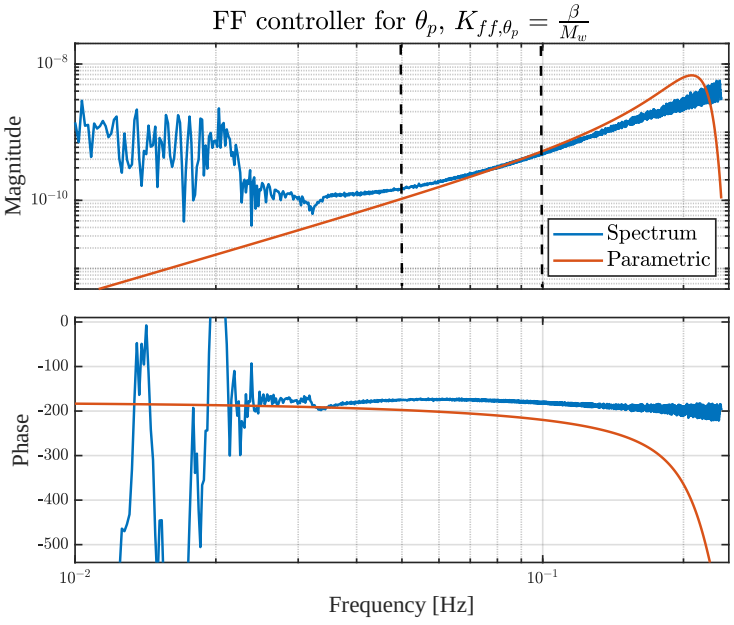

Figure 8. Bode plot of the optimal feedforward controller that targets the platform pitch motion. Blue: spectral estimate, Red: parametric controller.

Investigating Fig. 7 and Fig. 8, they show a good agreement between the spectral-based~~,~~ and the parametric FF controller within the frequency band of interest enclosed by the dashed vertical lines, which gives confidence in the fitted parametric controllers.

4 Results

In this section, the results from the experimental campaign are illustrated and discussed. The wave tank tests were performed at different conditions to properly assess the controller performance for ~~both objectives;~~ power regulation, and motion reduction. First the effectiveness of both controllers is discussed, before choosing to continue with the power regulation controller. The power regulator was tested at different wind speeds, turbulence intensities, significant wave heights and wave directions. Accordingly, each case would be treated separately. So, we will first look at the effect of varying the turbulence intensity, TI, at a certain wind speed. This is followed by varying the significant wave height, H_s, then the wave directional spreading parameter, s, before concluding with varying the wind speed, V. In each case, one of the parameters is varied, while the rest are kept constant. The different experiments that were performed are listed in Table 3:

https://doi.org/10.5194/wes-2023-180
Preprint. Discussion started: 16 January 2024

eawe european academy of wind energy
Open Access WIND ENERGY SCIENCE DISCUSSIONS

Table 3. Environmental conditions for the different experiments performed in the wave tank.

Case	V [m/s]	TI [%]	H_s [m]	T_p [s]	s [-]	Control objective [-]
Control objective	14	7.1	5	12	∞	[P_g, θ_p]
Variable TI	14	[0, 7.1, 13.8]	7	12	∞	P_g
Variable H_s	14	7.1	[5, 7, 9]	12	∞	P_g
Variable s	14	7.1	7	12	[15, 25, 60]	P_g
Variable V	[14, 17, 20]	7.1	7	12	∞	P_g

To clarify Table 3, we start by showing the performance of the FF controllers for both objectives; power regulation (P_g), and platform pitch motion reduction (θ_p). This is performed while keeping the other parameters constant. Afterwords, a decision is made to choose one of the two controllers to continue the rest of the campaign with. Following that decision, each of the remaining parameters is varied, while the rest are kept constant.

4.1 Control objective

We begin with illustrating the two different control objectives; power regulation, and platform motion reduction, each one at a time. At the end, we should be able to determine the potential of the wave feedforward control strategy, and what we can gain by applying such control.

For this comparison, the SIL experiment was performed at the same environmental conditions of wind and waves. Turbulent wind at 14 m/s with a TI of 7.1% was considered. Waves according to a JONSWAP spectrum, with significant wave height, ~~H_s~~, of 5 m, and peak period, ~~T_p~~, of 12 s were considered.

Figure 9 demonstrates the generator power, the collective blade pitch and the platform pitch time-domain responses together with their PSDs with the different controllers. As first, the experiment was performed only with the feedback controller as a baseline case. Afterwards, the feedforward controllers for both power regulation, and platform motion reduction, were added to the feedback, ~~respectively~~. We can see in the time response of the blade pitch signal the higher frequency ripples, corresponding to waves, oscillating about a lower frequency sinusoidal signal corresponding to the wind turbulence, which indicates that the feedforward controller, for both objectives, only picks up the higher frequency wave signals, while not reacting to the wind turbulence. This is also evident in the PSDs, where we see that in the wave frequency range (0.05-0.2 Hz) the generator power signal has less spectral content than the baseline case for the power regulation control objective, while there is no change at lower frequencies for both objectives. On the contrary, when the FF controller for the platform motion reduction objective is operational, the spectral content in the generator power signal slightly increases above the baseline, indicating more variance in the signal.

https://doi.org/10.5194/wes-2023-180
Preprint. Discussion started: 16 January 2024

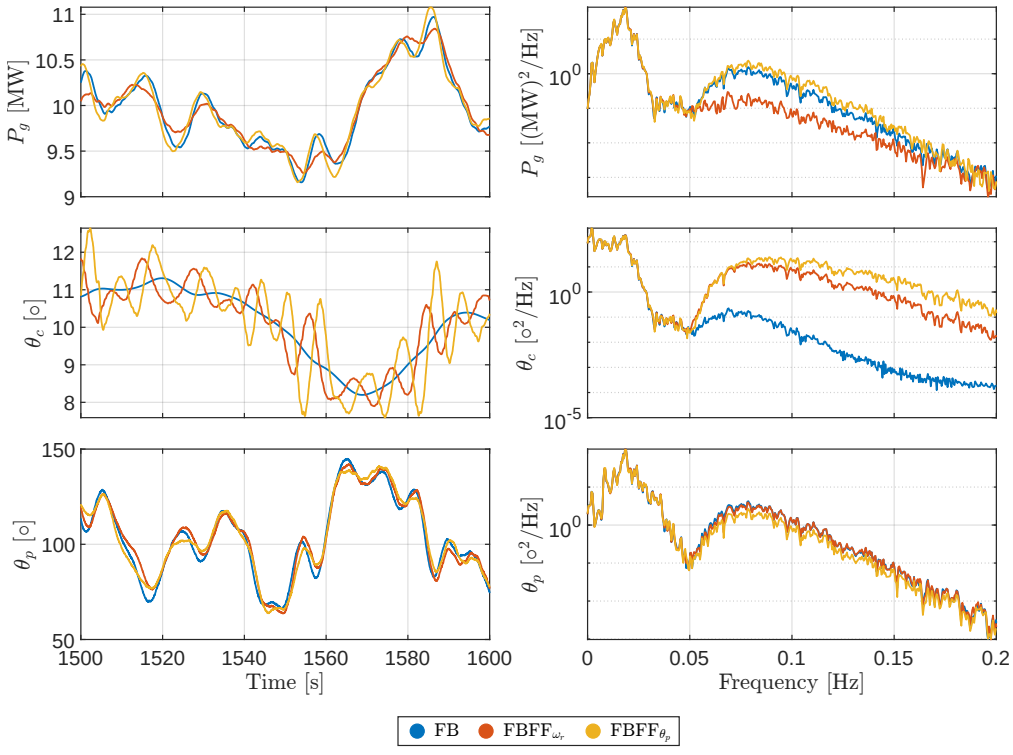

Figure 9. Generator power, blade pitch and platform pitch responses with and without wave feedforward control, at wind speed of 14 m/s, with a TI of 7.1%, and wave conditions of H_s = 5 m, and T_s = 12 s. The two feedforward controllers, for the objectives of power regulation and motion reduction~~,~~ are compared to the baseline feedback controller.

The PSDs in Fig. 9 also show that the power regulation objective leads to more reduction in the generator power variance with less blade pitch actuation than the other objective. So, we conclude that the reduction of the platform pitch motion requires a significantly large actuation for a smaller gain relative to the one for power regulation, which is ~~also~~ evident in Fig. 9, where the effect of the feedforward controller, FBFF$_{\theta_p}$, on the platform motion is minor, unlike the effect of FBFF$_{\omega_r}$ on the generator power.

In Fig. 10, the standard deviation, as a statistical metric illustrating the variation of a signal about its mean, is used to demonstrate the effect of the feedforward controller for both control objectives. In fact, Fig. 10 shows the percentage difference between the standard deviation of the signals with and without the FF control, which is normalised with respect to the baseline feedback standard deviation. As mentioned earlier in Fig. 9, FBFF$_{\omega_r}$ is mitigating the wave effects on the quality of the generator power, P_g, by reducing the rotor speed, ω_r, variations as illustrated in Fig. 10. The collective blade pitch, θ_c, variation increases for both FF controllers relative to the baseline case, which indicates that indeed the feedforward controller is active for both objectives, but the FF for power regulation requires almost half the blade pitch actuation needed by FBFF$_{\theta_p}$, and we even get more gain for the same control action. However, this is not the case for the platform motion reduction FF control, as the blade pitch variation about the mean value increases by almost 20% over the baseline case. Even though the blade pitch

https://doi.org/10.5194/wes-2023-180
Preprint. Discussion started: 16 January 2024

eawe european academy of wind energy
Open Access WIND ENERGY SCIENCE DISCUSSIONS

action is higher than in the baseline case, the FF control contribution reduces that of the feedback controller as it does not need to react to the wave disturbance anymore since the FF is taking care of that. The variation of the thrust force varies for both objectives, as for the FBFF$_{\omega_r}$, the thrust variance decreases below the baseline, which is not the case for FBFF$_{\theta_p}$. The thrust variation is reduced as a result of more blade pitching by FBFF$_{\omega_r}$ in order to regulate the rotor speed, while for FBFF$_{\theta_p}$, thrust is varied continuously to keep the platform motion in the pitch DOF as minimal as possible. As for the platform motion, we can say that the FF control in general has a positive effect on the platform motions as we see a reduction for both control objectives in most of the degrees of freedom (DOFs). Now that might vary from one DOF to another as we can see, for instance, there is a minor reduction in the surge, x_p, and pitch, θ_p, DOFs, while a significant reduction in sway, y_p, and roll, α_p, DOFs. For heave, z_p, and yaw, γ_p, DOFs, FBFF$_{\omega_r}$ and FBFF$_{\theta_p}$ lead to more oscillations, while their effect differs when it comes to yaw DOF. As FBFF$_{\omega_r}$ increases oscillations in platform yaw, while FBFF$_{\theta_p}$ reduces those fluctuations significantly. This is an extra effect from FBFF$_{\theta_p}$ since it was designed to mitigate the platform pitch, θ_p, oscillations only. FBFF$_{\omega_r}$ hardly affects the tower-base bending moment, $M_{TwrBs,y}$, as an insignificant increase is observed, which is not the case for FBFF$_{\theta_p}$ that leads to more tower-base loading. Regarding the mooring tension, T_{moor}, both FBFF$_{\omega_r}$ and FBFF$_{\theta_p}$ affect the mooring tension slightly, as FBFF$_{\omega_r}$ leads to a small reduction in the tension oscillation, while FBFF$_{\theta_p}$ causes a slight increase in the mooring tension.

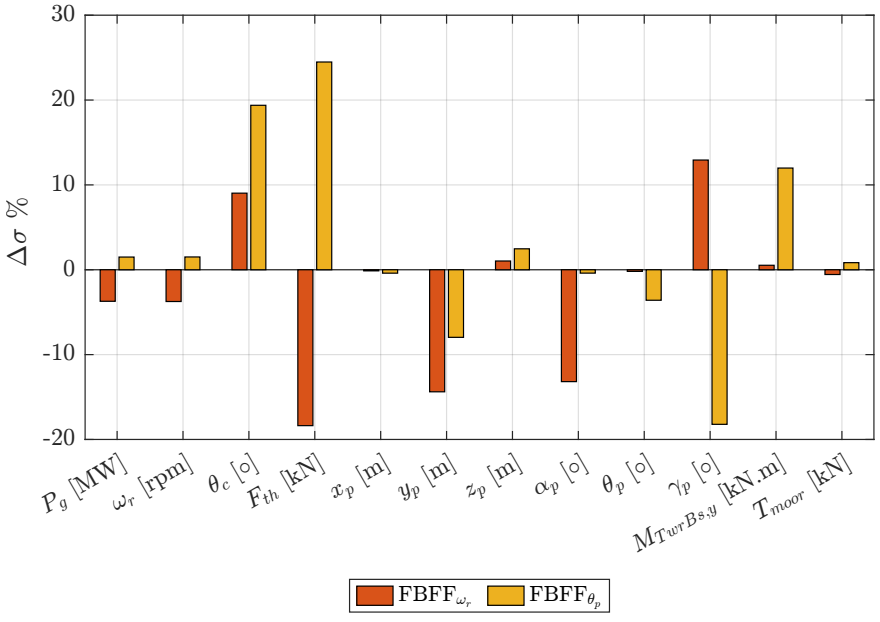

Figure 10. Normalised standard deviation percentage change of the two different control modes for different variables with respect to the baseline feedback case. All cases were held at wind speed of 14 m/s, with a TI of 7.1%, and wave conditions of H_s = 5 m, and T_s = 12 s.

According to Fig. 10, we can say that the platform motion alleviation objective requires a huge actuation effort, unlike the power regulation objective . As a result, we proceeded with the FF control for power regulation, FBFF$_{\omega_r}$, for the rest of the study.

https://doi.org/10.5194/wes-2023-180
Preprint. Discussion started: 16 January 2024

eawe european academy of wind energy
Open Access WIND ENERGY SCIENCE DISCUSSIONS

4.2 Effect of turbulence intensity variation

After showing the potential of FF control for both objectives, and observing that the platform pitch motion reduction FF control requires huge actuation, the remaining experimental results are based on the power regulator FF. We start with investigating the effectiveness of the FF controller while varying the turbulent intensity. The experimental results at wind speed 14 m/s were chosen for this discussion. Fig. 11, Fig. 12 and Fig. 13 clearly illustrate the performance of the FF control. In Fig. 11 the effect of waves on the generator power is reduced compared to the FB only cases, as there is a reduction at all the turbulent intensities, within the wave frequency range (0.05-0.2 Hz). This is depicted in the Power Spectral Density (PSD) of Fig. 11 where the addition of FF control reduces the energy within the wave energy band. However, it has no effect within the low-frequency band corresponding to wind turbulence, which is to be expected since the controller's bandwidth is targeting the wave frequency range only.

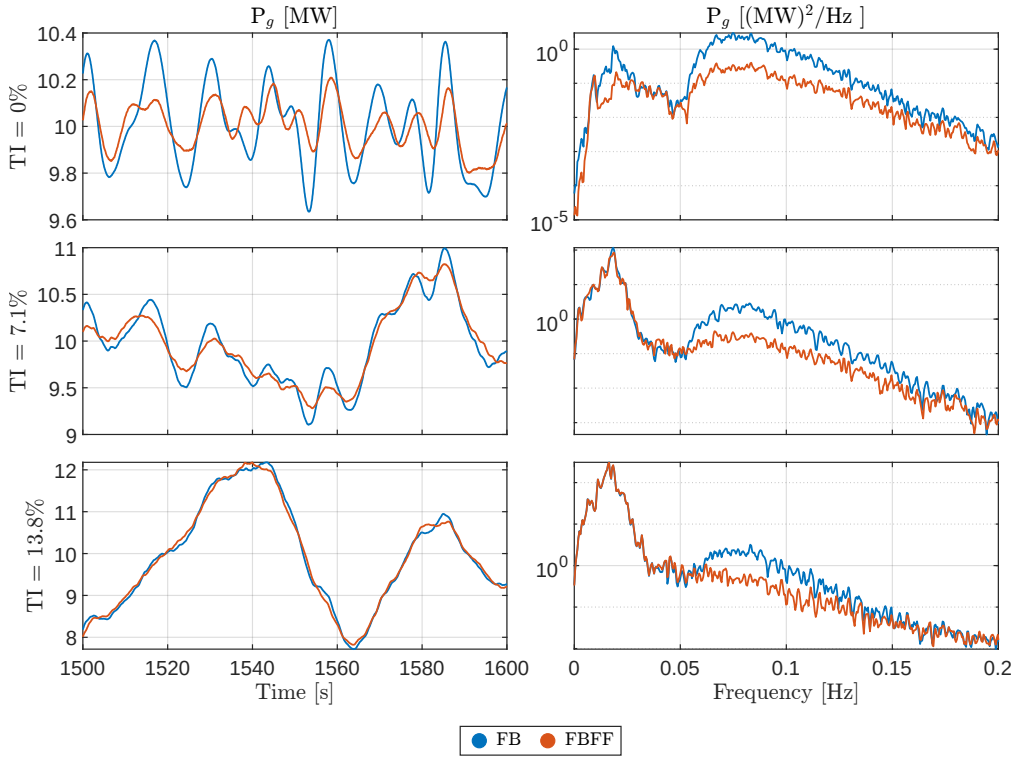

Figure 11. Generator power response with and without wave feedforward control, at wind speed of 14 m/s, varying from steady wind at 0% TI to turbulent wind at a TI of 7.1% and 13.8%.

Increasing the turbulence intensity has a direct effect on increasing the variance of the depicted signals. We can clearly observe how the time traces are dominated by the high frequency sinusoids, relevant to wave frequency band, ~~in steady wind,~~ while the low frequent sinusoids, relevant to wind turbulence, dominate as the TI increases ~~leading~~ to increasing the peak-to-peak value about the mean of the signal, indicating an increase in the variance of the signal. This can also be confirmed by

https://doi.org/10.5194/wes-2023-180
Preprint. Discussion started: 16 January 2024

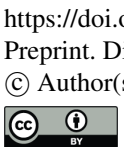

eawe european academy of wind energy
Open Access WIND ENERGY SCIENCE DISCUSSIONS

the PSD ~~plots,~~ where there is more spectral content in the low frequency bandwidth than the bandwidth related to the waves. In steady wind, we can observe a reduction in the generator power variation. However, once the ~~wind inflow becomes more realistic, and~~ wind turbulence increases, the reduction in the generator power oscillations is not as significant. This indicates that the wind turbulence, lying in the low-frequency band, dominates the global dynamic response even though the wave FF controller is taking care of oscillations caused by the waves in the high-frequency band.

Figure 12 illustrates the platform pitch response at different turbulence intensities. In Fig. 12, we see that the FF controller has no authority on the platform motions in the wave band, which is reasonable since this controller is mainly aimed at reducing power fluctuations. Also, for the TI effect, we see a clear domination of the wind turbulence.

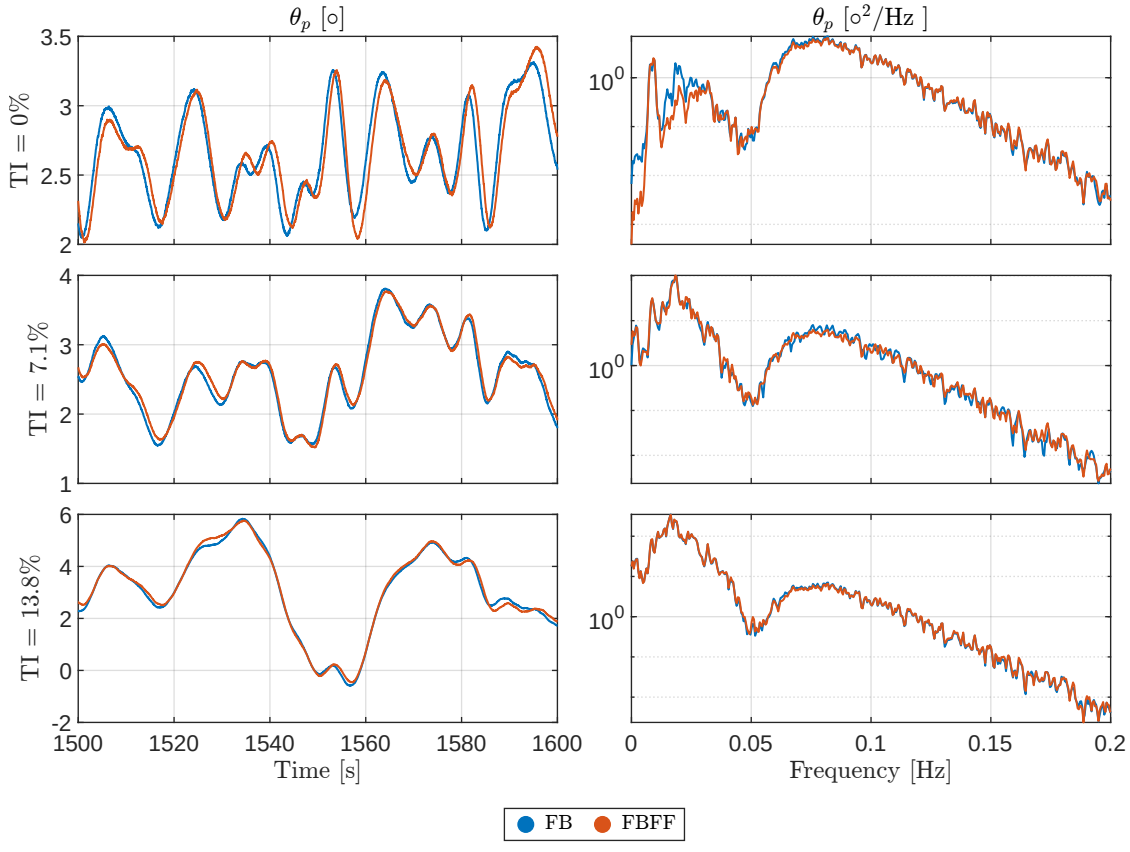

Figure 12. Platform pitch response with and without wave feedforward control, at wind speed of 14 m/s, varying from steady wind at 0% TI to turbulent wind at a TI of 7.1% and 13.8%.

As for the collective blade pitch angle in Fig. 13, the pitch actuator is clearly active in the wave frequency range with the FF control compared to the FB controller. We see that the FB controller is only reacting to the low frequency wind turbulence, while not considering the wave disturbance because of the negative damping implications that would happen if the bandwidth of the FB controller is increased (Nielsen et al., 2006; Jonkman, 2008; van der Veen et al., 2012; Fischer, 2013; Fleming et al.,

https://doi.org/10.5194/wes-2023-180
Preprint. Discussion started: 16 January 2024

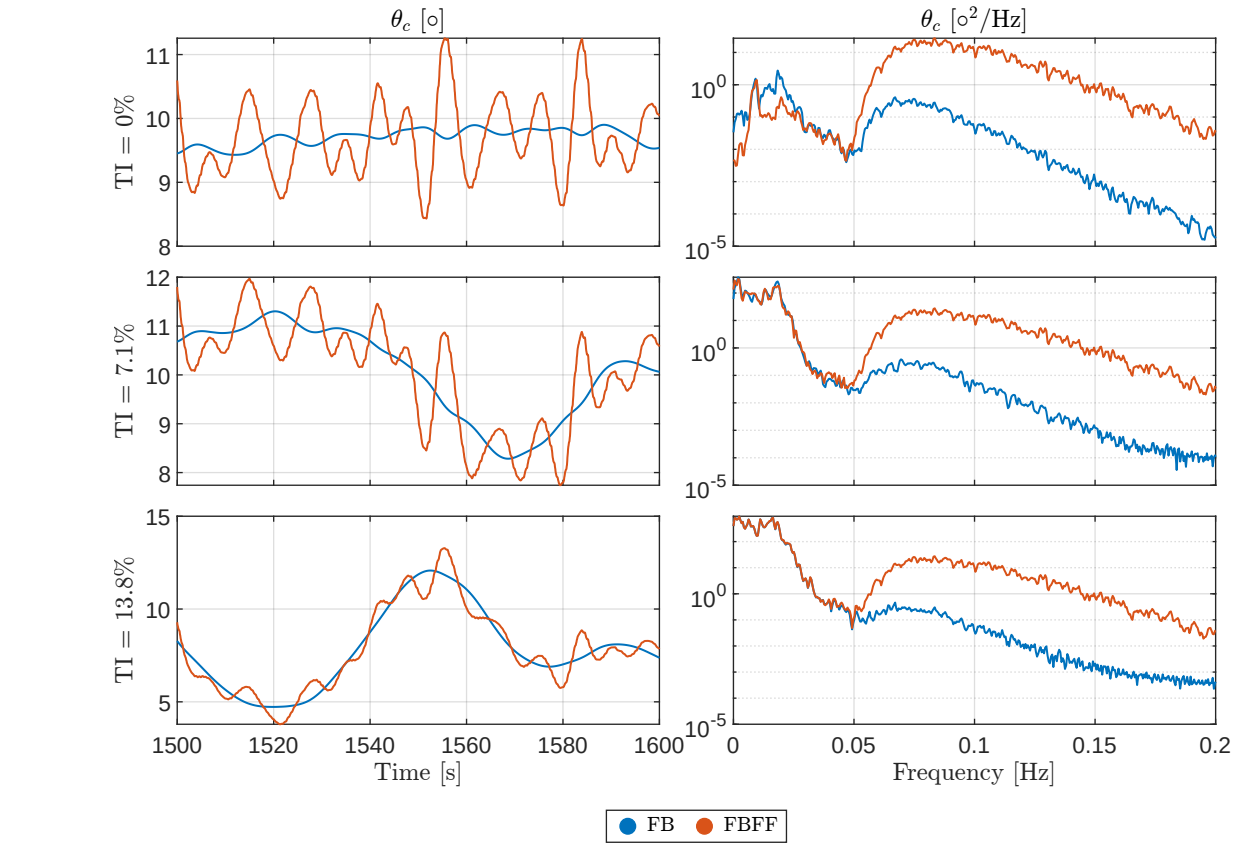

Figure 13. Collective blade pitch angle with and without wave feedforward control, at wind speed of 14 m/s, varying from steady wind at 0% TI to turbulent wind at a TI of 7.1% and 13.8%.

~~Regarding~~ the Standard Deviation (SD) of the signals is used to quantify the effect of the FF control on the different variables as shown in Fig. 14. It is fair to mention that the figure illustrates the difference between the FF control with respect to the baseline FB controller in steady wind case. The effect of including FF control can already be seen as the main objective of the FF controller is to regulate the generator power, P_g. However, the focus in this subsection is on the effectiveness of the FF strategy at different wind inflow turbulent intensity conditions. It is striking to see how the wind dominates the waves as the turbulence intensity increases, as the reduction in the generator power fluctuations decreases with the increase in the turbulence intensity. Thus, we can conclude that the FF strategy is indeed effective for improving the power quality, but as the turbulence intensity increases, the effectiveness of the FF diminishes. Furthermore, the effect of the turbulence intensity on the platform motion varies from one DOF to another, and there is no clear trend for the different DOFs.

https://doi.org/10.5194/wes-2023-180
Preprint. Discussion started: 16 January 2024

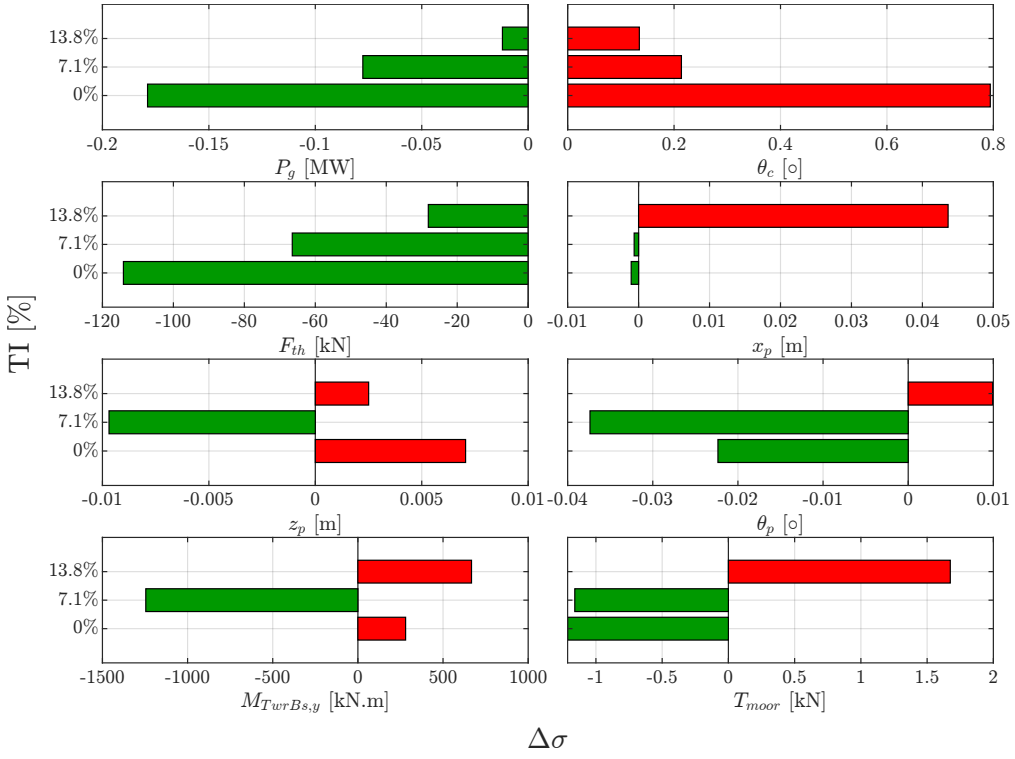

Figure 14. Standard deviation change with wave feedforward control relative to the baseline feedback control, at wind speed of 14 m/s, varying from steady wind at 0% TI to turbulent wind at a TI of 7.9% and 13%.

4.3 Effect of significant wave height variation

Varying the significant wave height has, without a doubt, effects on the control performance. As the disturbance TF accounts for the mapping from the wave excitation forces, as a disturbance input, to ~~either~~ the rotor speed ~~or the platform pitch, as an output depending on the control objective~~. By wave excitation forces, we are referring to the first order wave forces based on linear wave theory (Newman, 2018), where there is a direct transfer from the wave height to the first order wave excitation forces through the transfer functions known as the Response Amplitude Operators (RAOs). To have a deeper look at this subject, different wave conditions were applied, where different significant wave heights were considered, while keeping both the peak period and the wind speed constant. This is in addition to having long-crested unidirectional waves.

https://doi.org/10.5194/wes-2023-180
Preprint. Discussion started: 16 January 2024

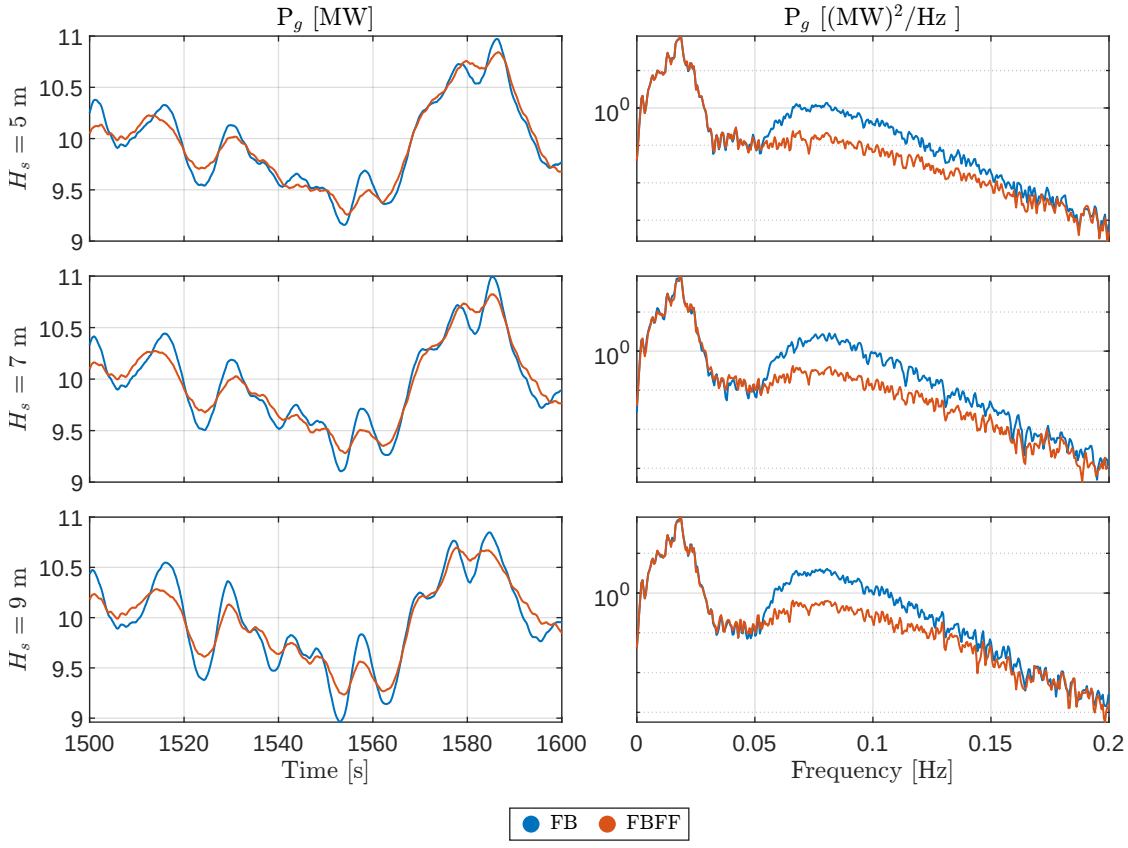

Figure 15. Generator power responses with and without wave feedforward control, at a turbulent wind speed of 14 m/s with a 7.1% TI, and unidirectional waves at $S = \infty$, and T_p = 12 s, but at different significant wave heights, H_s.

Looking at Fig. 16, apart from the FF control operating as expected, we can see how the amplitude of the generator power signal increases as waves get bigger, which corresponds to an increase in energy in the PSDs for the corresponding signals. This rise in amplitude can also be observed in the blade pitch signal to maintain the rotor speed as close to its rated value as possible.

https://doi.org/10.5194/wes-2023-180
Preprint. Discussion started: 16 January 2024

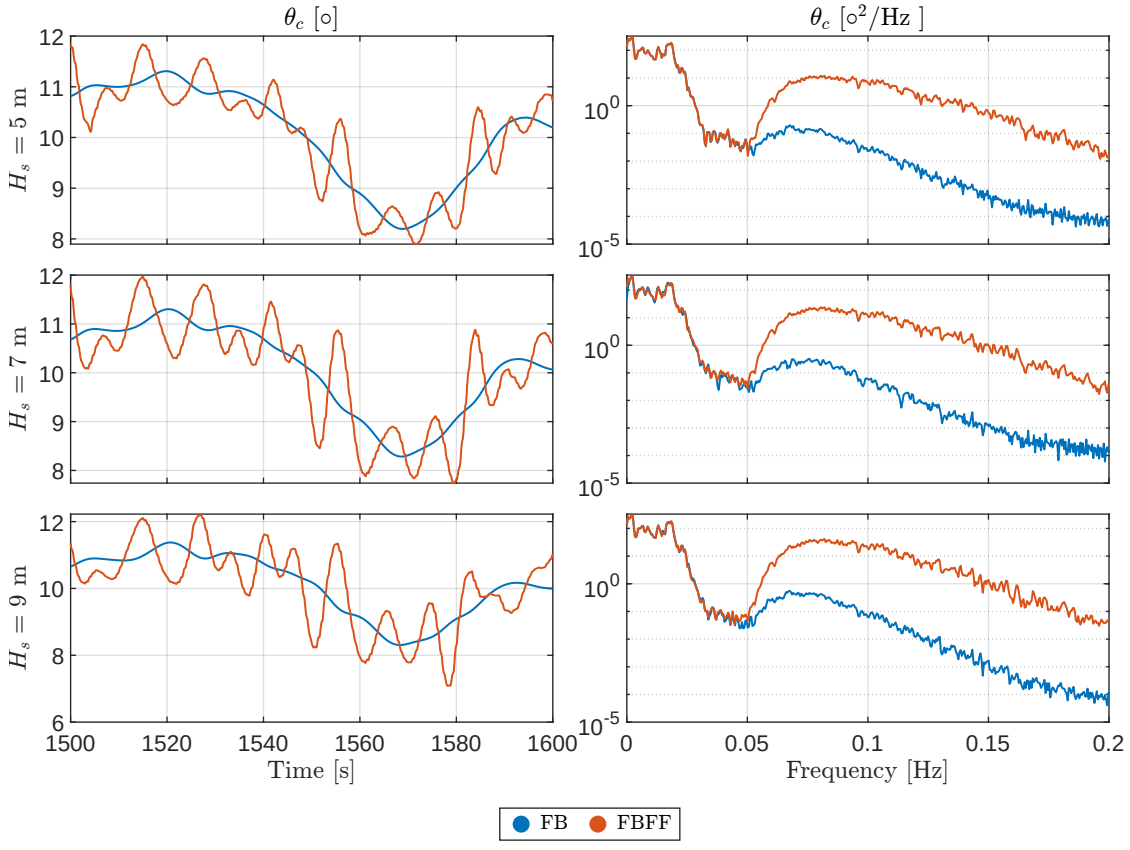

Figure 16. Collective blade pitch responses with and without wave feedforward control, at a turbulent wind speed of 14 m/s with a 7.1% TI, and unidirectional waves at $S = \infty$, and T_p = 12 s, but at different significant wave heights, H_s.

Figure 17 summarises the effect of varying the significant wave height on the different variables of interest. It is pretty clear how the FF controller reacts to waves; the bigger they get the stronger the FF control action is. This is illustrated in the generator power, and the blade pitch signals. On the contrary, we see a rise in the fluctuations in the thrust force as the significant wave height becomes higher.

As for the platform motion, each DOF has a different sensitivity to the wave height variation, as there is no clear trend they are following all together. Furthermore, there is not even a trend for every DOF separately. We see, for instance, that the fluctuations in the surge DOF significantly decreases with the FF control compared to the baseline FB controller at $H_s = 5$ m, while as the wave height increases, the percentage difference in the standard deviation goes from negative to positive at $H_s = 9$ m indicating that the power regulation FF control leads to higher surge displacements at bigger waves. Concerning heave and pitch DOFs, we observe that at $H_s = 7$ m in particular, there is a considerable alleviation in the oscillations of both signals with respect to the baseline FB control. However, an increase in the platform heave oscillations can be seen for the other two wave heights, while a mitigation in the platform pitch fluctuations.

https://doi.org/10.5194/wes-2023-180
Preprint. Discussion started: 16 January 2024

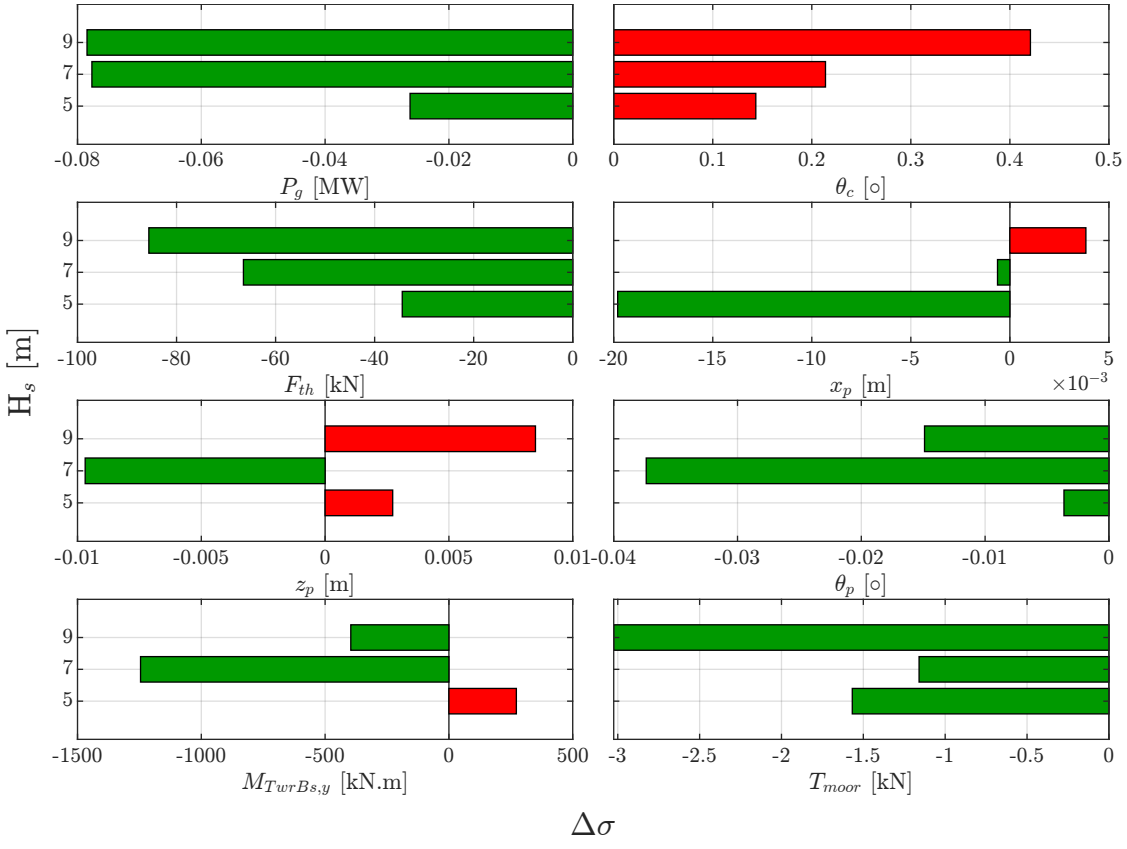

Figure 17. Standard deviation change of different variables of interest with wave feedforward control, at a turbulent wind speed of 14 m/s with a 7.1% TI, and waves of T_p = 12 s, but at different significant wave heights, H_s. The bars illustrate the difference in standard deviation with the FF control compared to the baseline case at each significant wave height.

4.4 Effect of wave directional spreading

After investigating the effect of varying the turbulence intensities, and the significant wave height, we move on to the effect of the wave directional spreading on the different variables of interest with the FF control present. For this part of the experimental campaign, waves were generated at a significant wave height, $H_s = 7$ m, and a peak period, T_p = 12 s, but at a different directional spreading parameter, where it was varied from a low value corresponding to short-crested waves of a multidirectional nature, to higher values that correspond to long-crested waves that act in a more unidirectional manner.

Starting with Fig. 18, where the generator power is depicted, it can be observed that even though the disturbance TF, used in the FF control synthesis, was identified based on unidirectional waves, yet the FF controller is working well also in multidirectional waves, which is evident in the time history and the PSD. As for the different directional spreading parameter cases whether with FB cases only or FBFF cases, we can not really detect a big influence of the wave directional spreading on the generator power signal, as the amplitudes at each time instant, or frequency, almost do not change.

https://doi.org/10.5194/wes-2023-180
Preprint. Discussion started: 16 January 2024

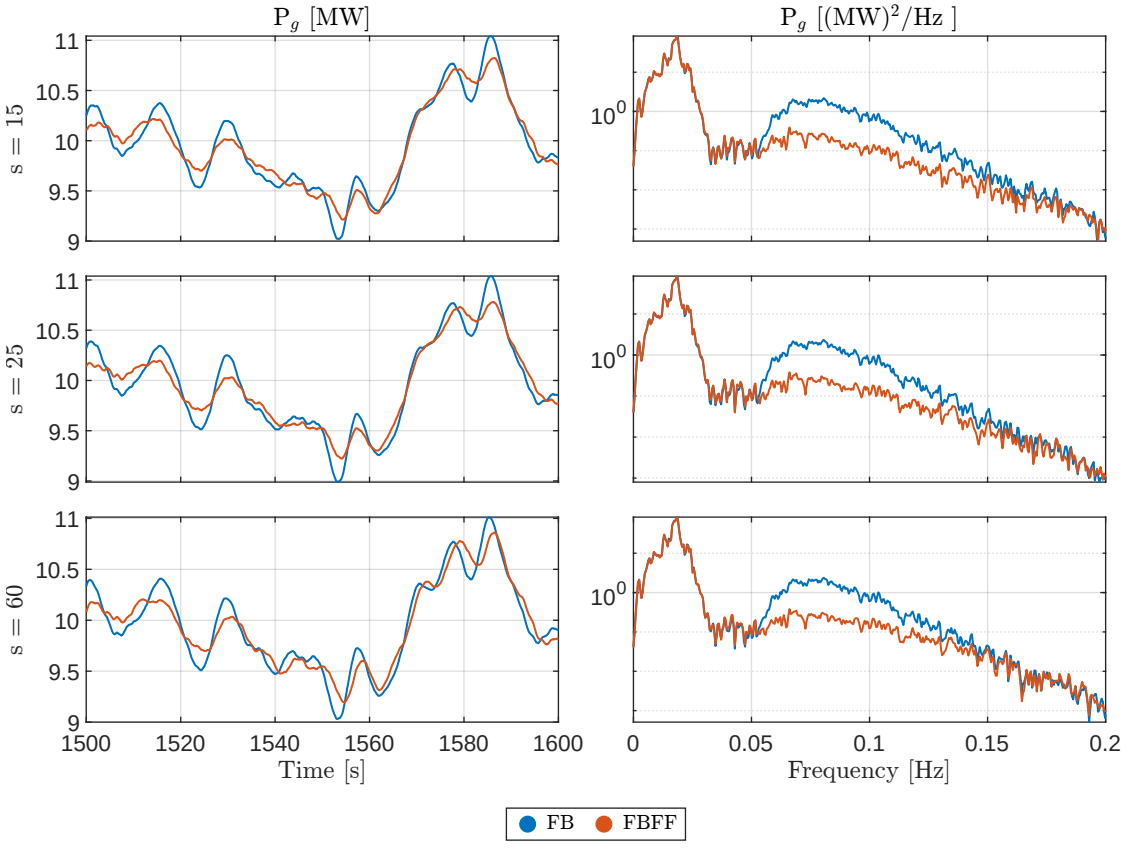

Figure 18. Generator power response with and without wave feedforward control, at a turbulent wind speed of 14 m/s with a 7.1% TI, and waves with H_s = 7 m, and T_p = 12 s, but with different directional spreading paramter, S, varying from short to long crested waves.

Moving to Fig. 19, again, the activity of the FF controller within different wave directional conditions is clear, and again, the amplitudes of the blade pitch signal do not differ too much from each other.

https://doi.org/10.5194/wes-2023-180
Preprint. Discussion started: 16 January 2024

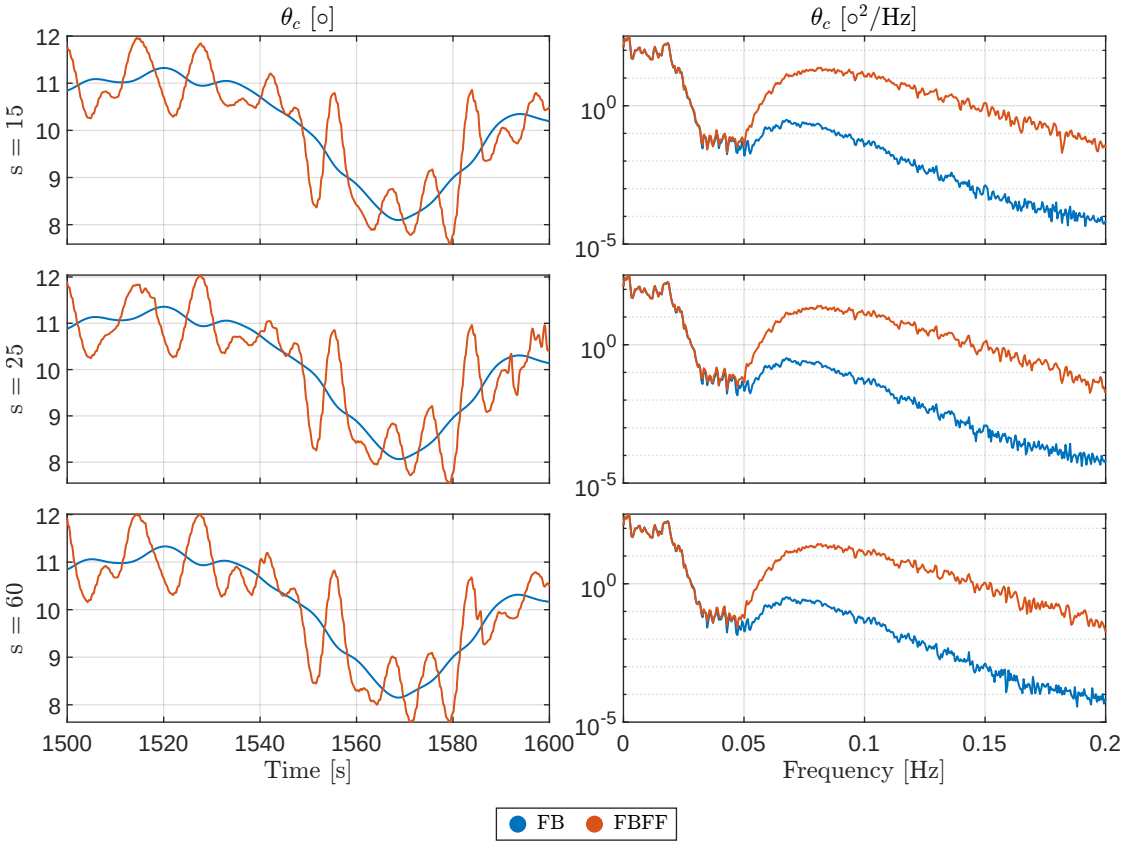

Figure 19. Collective blade pitch response with and without wave feedforward control, at a turbulent wind speed of 14 m/s with a 7.1% TI, and waves with H_s = 7 m, and T_p = 12 s, but with different directional spreading paramter, S, varying from short to long crested waves.

The wave directionality results are summarised in Fig. 20. We see that in short-crested waves, which are the ones with low spreading parameter, the effectiveness of the FF control is slightly reduced compared to the long-crested waves case. This is because the alleviation of the power fluctuations is less in short-crested waves. Consequently, the variance in the thrust force reduces. The sole reason of the thrust variation reduction is due to the introduction of the FF control that is trying to regulate the power, and in the process changes the thrust force continuously in order to maintain a power signal that is free of the wave fluctuations.

Again, there is no specific trend for the platform motions, as we see a different effect at each spreading parameter for every DOF. Also, the different DOFs do not agree on a certain behaviour at every spreading parameter. We see the surge decreasing at short-crested, then increasing, before decreasing again. The heave decreases slightly before increasing all the way. The platform pitch is always less oscillatory than the baseline FB case, but this reduction in oscillations seems to vary in a random manner, as the reduction is maximum at short-crested waves, then decreases as the wave spreading decreases (s increases), before increasing again slightly as the waves become more long-crested.

https://doi.org/10.5194/wes-2023-180
Preprint. Discussion started: 16 January 2024

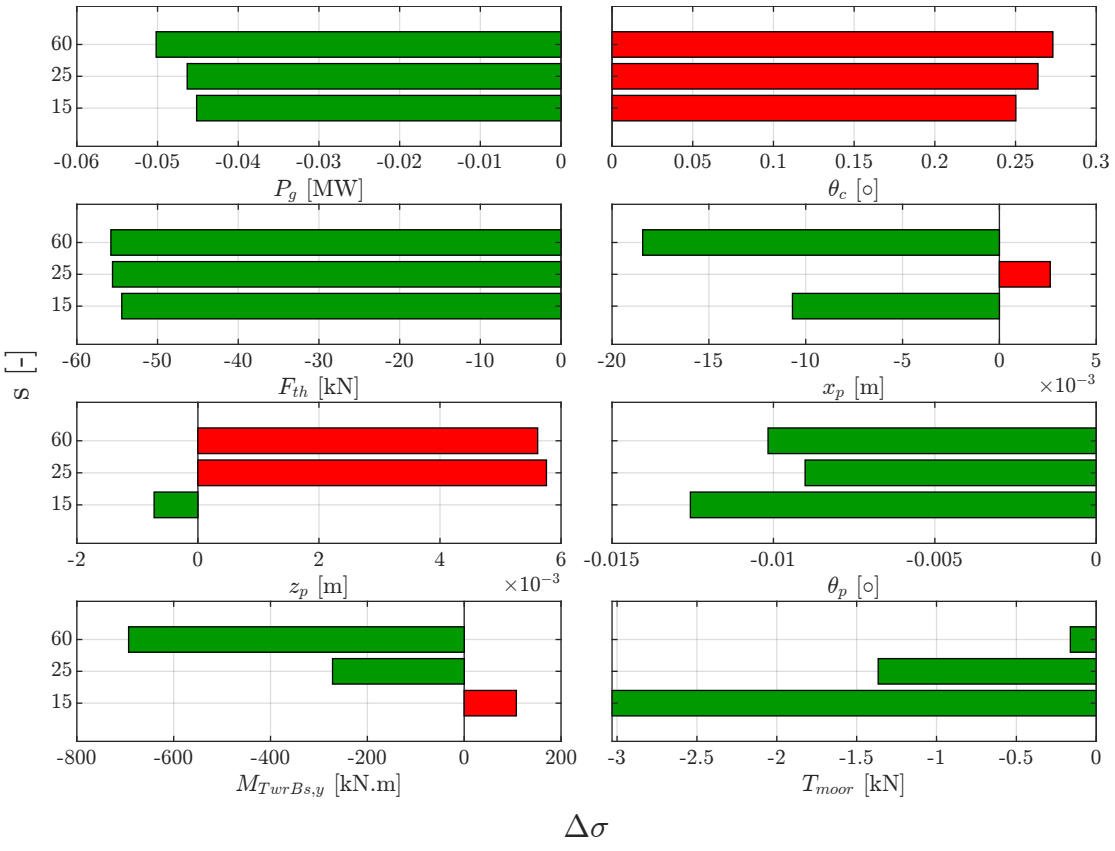

Figure 20. Normalised standard deviation percentage change of different variables of interest with wave feedforward control, at a turbulent wind speed of 14 m/s with a 7.1% TI, and waves with H_s = 7 m, and T_p = 12 s, but with different directional spreading paramter, S, varying from short-crested, at S = 15, to longer crested waves at S = 60. The bars illustrate the difference in standard deviation with the FF control compared to the baseline case at each directional spreading parameter.

4.5 Controller performance at different wind speeds

In this subsection, we show the control performance when the wind speed varies. Initially, the controller was synthesized at a single operating point at wind speed of 16 m/s. Consequently, the controller might be expected not perform optimally. However, Fig. 21 suggests otherwise, as it shows the controller efficiently operating at different wind speeds. This is clear in both the time response, where we observe a decent reduction in the peak-to-peak amplitudes, as well as the spectral content in the PSDs.

This gives confidence in the controller that it is robust enough to handle the non-linear dynamics of the FOWTs without the need for gain scheduling even though it was synthesized for a single operating point. Of course having a gain-scheduled controller would ensure that the controller is performing optimally at each operating point across the spectrum of the operating wind speeds of the wind turbine~~, yet sometimes~~ having a sub-optimal controller is preferred to have a compromise between performance and control effort.

https://doi.org/10.5194/wes-2023-180
Preprint. Discussion started: 16 January 2024

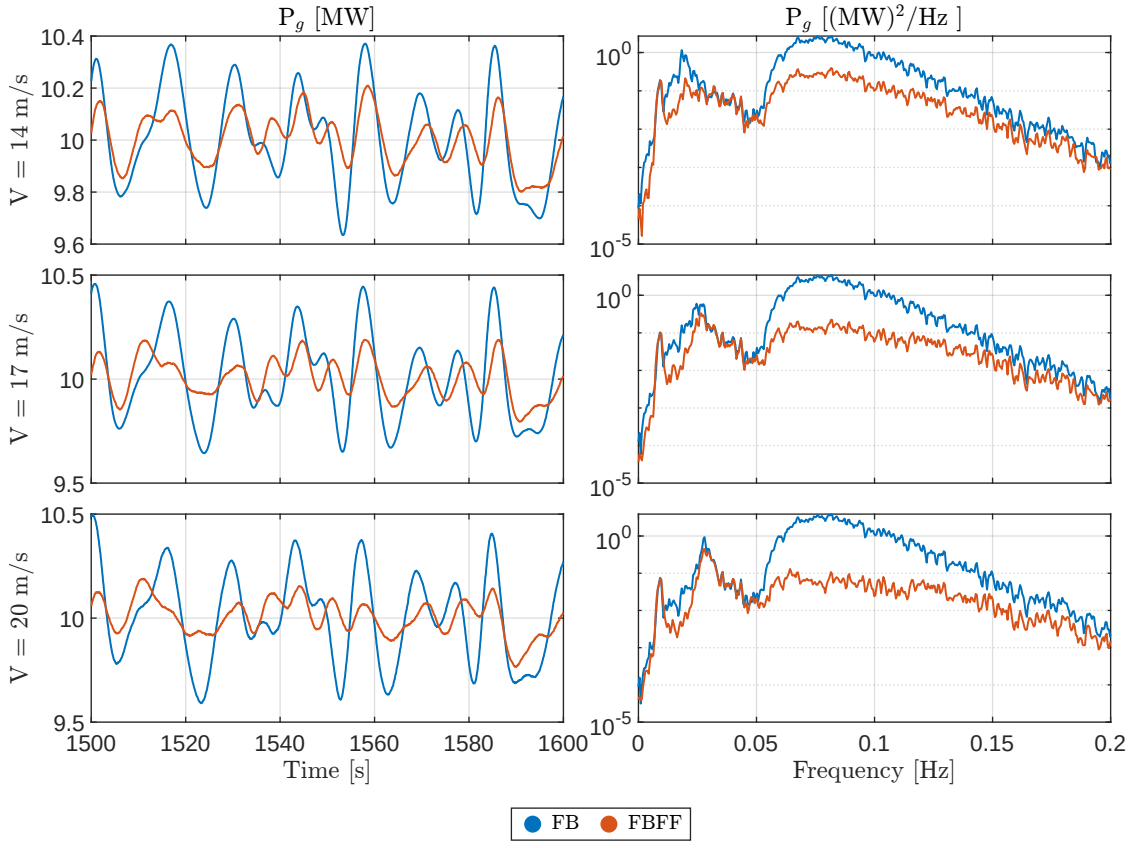

Figure 21. Generator power response with and without wave feedforward control, at different steady wind speeds at 14 m/s, 17 m/s and 20 m/s, and long-crested waves with H_s = 7 m, T_p = 12 s, and S = ∞.

5 Conclusions

Successful wave tank experiments were conducted to evaluate the feedforward control strategy benefits in terms of the structural loads and the power quality of the floating wind turbine components. It was found that the effectiveness of the wave feedforward controller for reducing the power fluctuations is higher than the one for decreasing the platform pitch ~~motion. As,~~ the FF controller for generator power requires less actuation than the FF controller for the platform pitch motion, and the reduction in the generator power oscillations is greater than the alleviation in the platform pitch motion. The experiments went on to investigate the performance of the feedforward control within environmental conditions, as well as how these conditions affect the turbine dynamics in general. Subsequently, some experiments were performed at different wind turbulence intensities, others at varying significant wave heights, and others at contrasting wave spreading conditions.

The wave feedforward strategy was indeed proven to be operational and effective at different environmental conditions. However, we concluded that as the turbulence intensity increases, the wind dominates and the effectiveness of the FF control diminishes. As for varying significant wave heights, as the waves get bigger, the reponses of the different DOFs of the platform

https://doi.org/10.5194/wes-2023-180
Preprint. Discussion started: 16 January 2024

motion do not follow a clear trend, however, it is rather random. While for different wave spreading parameters, it was shown that the power fluctuations are higher in case of short-crested waves than in long-crested ones. However, the difference is rather insignificant, which indicates that the main source of fluctuations is the fore-aft direction.

In short, the wave feedforward control strategy is effective when it comes to alleviating the effects of the wave forces on the FOWT, whereas, wave FF control requires significant amount of actuation to minimise the platform pitch motion, which makes such a technology unfavourable for that objective.

Author contributions. AH conceptualisation, methodology, investigation, writing – original daft under the super-vision of PN and JWVW. VL, FB, YP designed the wave tank experiment. The insights and conclusion presented in this paper are the results of extensive discussions among the coauthors. All coauthors thoroughly reviewed the article.

Competing interests. At least one of the (co-)authors is a member of the editorial board of Wind Energy Science.

Acknowledgements. This project is part of the FLOATECH project. The research presented in this paper has received funding from the European Union's Horizon 2020 research and innovation programme under grant agreement no. 101007142.

https://doi.org/10.5194/wes-2023-180
Preprint. Discussion started: 16 January 2024

eawe european academy of wind energy
Open Access WIND ENERGY SCIENCE DISCUSSIONS

References

Al, M.: Feedforward control for wave disturbance rejection on floating offshore wind turbines, 2020.

Al, M., Fontanella, A., van der Hoek, D., Liu, Y., Belloli, M., and van Wingerden, J. W.: Feedforward control for wave disturbance rejection on floating offshore wind turbines, in: Journal of Physics: Conference Series, vol. 1618, p. 022048, IOP Publishing, 2020.

Arnal, V.: Modélisation expérimentale d'une éolienne flottante par une approche sofware-in-the-loop, Ph.D. thesis, http://www.theses.fr/2020ECDN0037, 2020.

Bak, C., Zahle, F., Bitsche, R., Kim, T., Yde, A., Henriksen, L. C., Hansen, M. H., Blasques, J. P. A. A., Gaunaa, M., and Natarajan, A.: The DTU 10-MW reference wind turbine, in: Danish wind power research 2013, 2013.

Chen, C., Ma, Y., and Fan, T.: Review of model experimental methods focusing on aerodynamic simulation of floating offshore wind turbines, Renewable and Sustainable Energy Reviews, 157, 112 036, 2022.

European Commission: European Wind Power Action Plan., https://energy.ec.europa.eu/system/files/2023-10/COM_2023_669_1_EN_ACT_part1_v8.pdf, (accessed: 16-11-2023), 2023.

Fischer, B.: Reducing rotor speed variations of floating wind turbines by compensation of non-minimum phase zeros, 7, 413–419, https://doi.org/10.1049/iet-rpg.2012.0263, 2013.

Fleming, P. A., Pineda, I., Rossetti, M., Wright, A. D., and Arora, D.: Evaluating methods for control of an offshore floating turbine, in: International Conference on Offshore Mechanics and Arctic Engineering, vol. 45547, p. V09BT09A019, American Society of Mechanical Engineers, 2014.

Fontanella, A., Al, M., van Wingerden, J., and Belloli, M.: Model-based design of a wave-feedforward control strategy in floating wind turbines, Wind Energy Science, 6, 885–901, https://doi.org/10.5194/wes-6-885-2021, 2021.

Fontanella, A., Facchinetti, A., Daka, E., and Belloli, M.: Modeling the coupled aero-hydro-servo-dynamic response of 15 MW floating wind turbines with wind tunnel hardware in the loop, Renewable Energy, p. 119442, 2023.

Hegazy, A., Naaijen, P., and van Wingerden, J. W.: A novel control architecture for floating offshore wind turbines, in: IFAC 22nd World Congress, 2023a.

Hegazy, A., Naaijen, P., and van Wingerden, J.-W.: Wave Feedforward Control for Large Floating Wind Turbines, in: 2023 IEEE Conference on Control Technology and Applications (CCTA), pp. 593–598, IEEE, 2023b.

Jonkman, J.: Influence of Control on the Pitch Damping of a Floating Wind Turbine, in: 46th AIAA Aerospace Sciences Meeting and Exhibit, American Institute of Aeronautics and Astronautics, https://doi.org/10.2514/6.2008-1306, 2008.

Kim, I.-C., Ducrozet, G., Bonnefoy, F., Leroy, V., and Perignon, Y.: Real-time phase-resolved ocean wave prediction in directional wave fields: Enhanced algorithm and experimental validation, Ocean Engineering, 276, 114 212, 2023.

Kim, I.-C., Ducrozet, G., Leroy, V., Bonnefoy, F., Perignon, Y., and Bourguignon, S.: A real-time wave prediction in directional wave fields: Strategies for accurate continuous prediction in time, Ocean Engineering, 291, 116 445, 2024a.

Kim, I.-C., Ducrozet, G., Leroy, V., Bonnefoy, F., Perignon, Y., and Delacroix, S.: Numerical and experimental investigation on deterministic prediction of ocean surface wave and wave excitation force, Applied Ocean Research, 142, 103 834, 2024b.

Lemmer, F., Yu, W., Schlipf, D., and Cheng, P. W.: Robust gain scheduling baseline controller for floating offshore wind turbines, 23, 17–30, https://doi.org/10.1002/we.2408, 2020.

Ma, Y., Sclavounos, P. D., Cross-Whiter, J., and Arora, D.: Wave forecast and its application to the optimal control of offshore floating wind turbine for load mitigation, Renewable Energy, 128, 163–176, 2018.

https://doi.org/10.5194/wes-2023-180
Preprint. Discussion started: 16 January 2024

Marten, D.: Qblade Website, http://www.q-blade.org, (accessed: 02-02-2023), 2023.

Naaijen, P. and Wijaya, A. P.: Phase Resolved Wave Prediction From Synthetic Radar Images, vol. Volume 8A: Ocean Engineering of *International Conference on Offshore Mechanics and Arctic Engineering*, https://doi.org/10.1115/OMAE2014-23470, 2014.

Navalkar, S. T., van Wingerden, J. W., Fleming, P. A., and Van Kuik, G.: Integrating robust lidar-based feedforward with feedback control to enhance speed regulation of floating wind turbines, in: 2015 American Control Conference (ACC), pp. 3070–3075, IEEE, 2015.

Newman, J. N.: Marine hydrodynamics, The MIT press, 2018.

Nielsen, F. G., Hanson, T. D., and Skaare, B.: Integrated Dynamic Analysis of Floating Offshore Wind Turbines, pp. 671–679, ASMEDC, https://doi.org/10.1115/OMAE2006-92291, 2006.

Raach, S., Schlipf, D., Sandner, F., Matha, D., and Cheng, P. W.: Nonlinear model predictive control of floating wind turbines with individual pitch control, in: 2014 American Control Conference, pp. 4434–4439, https://doi.org/10.1109/ACC.2014.6858718, 2014.

Saenz-Aguirre, A., Ulazia, A., Ibarra-Berastegi, G., and Saenz, J.: Floating wind turbine energy and fatigue loads estimation according to climate period scaled wind and waves, Energy Conversion and Management, 271, 116 303, 2022.

Schlipf, D., Schlipf, D. J., and Kühn, M.: Nonlinear model predictive control of wind turbines using LIDAR, Wind Energy, 16, 1107–1129, https://doi.org/https://doi.org/10.1002/we.1533, 2013.

Schlipf, D., Fleming, P., Haizmann, F., Scholbrock, A., Hofsäß, M., Wright, A., and Cheng, P. W.: Field testing of feedforward collective pitch control on the CART2 using a nacelle-based lidar scanner, in: Journal of Physics: Conference Series, vol. 555, p. 012090, IOP Publishing, 2014.

Schlipf, D., Lemmer, F., and Raach, S.: Multi-variable feedforward control for floating wind turbines using lidar, in: ISOPE International Ocean and Polar Engineering Conference, pp. ISOPE–I, ISOPE, 2020.

Scholbrock, A., Fleming, P., Fingersh, L., Wright, A., Schlipf, D., Haizmann, F., and Belen, F.: Field testing LIDAR-based feed-forward controls on the NREL controls advanced research turbine, in: 51st AIAA Aerospace Sciences Meeting Including the New Horizons Forum and Aerospace Exposition, p. 818, 2013.

van der Veen, G., van Wingerden, J. W., Bergamasco, M., Lovera, M., and Verhaegen, M.: Closed-loop subspace identification methods: an overview, IET Control Theory & Applications, 7, 1339–1358, 2013.

van der Veen, G. J., Couchman, I. J., and Bowyer, R.: Control of floating wind turbines, in: 2012 American Control Conference (ACC), pp. 3148–3153, IEEE, https://doi.org/10.1109/ACC.2012.6315120, 2012.